


 Cite this: *RSC Adv.*, 2023, **13**, 15126

 Received 23rd February 2023  
 Accepted 11th May 2023

 DOI: 10.1039/d3ra01216f  
[rsc.li/rsc-advances](http://rsc.li/rsc-advances)

## Red, green, and blue radio-luminescent polymer dots doped with heteroleptic tris-cyclometalated iridium complexes†

Zouyue Liu,<sup>‡,a</sup> Hieu Thi Minh Nguyen,<sup>‡,b</sup> Daiki Asanuma,<sup>a</sup> Sachiko Tojo,<sup>a</sup> Minoru Yamaji,<sup>ID, c</sup> Kiyohiko Kawai,<sup>ID, ad</sup> Guillem Pratx,<sup>ID, \*b</sup> Mamoru Fujitsuka,<sup>ID, \*ae</sup> and Yasuko Osakada,<sup>ID, \*aef</sup>

In this study, we synthesized radioexcitable luminescent polymer dots (**P-dots**) doped with heteroleptic tris-cyclometalated iridium complexes that emit red, green, and blue light. We investigated the luminescence properties of these **P-dots** under X-ray and electron beam irradiation, revealing their potential as new organic scintillators.

### Introduction

Radiation is widely used in medicine, industry, and scientific research.<sup>1,2</sup> For example, it is used in medical applications such as imaging and radiotherapy.<sup>3</sup> Among these medical applications, linear accelerators are used to deliver radiation, including hard X-rays and electron beams, to visualize and induce cell death in targeted areas.<sup>4</sup> The advantages of using X-rays and electron beams include their high biological permeability, which allows non-invasive imaging, high resolution and is already used in many clinical settings.<sup>5</sup> There is substantial interest in using these technologies to develop novel imaging and therapeutic modalities by using photo-functional nanomaterials. In fact, recent studies have demonstrated the potential applications of radiation for photodynamic therapy<sup>6</sup> and optogenetics<sup>7,8</sup> by using photo-functional materials. Regarding photo-functional (e.g., radio-luminescent) nanomaterials for photo-induced therapeutic applications,

scintillators are commonly used as the light-emitting materials.<sup>9</sup> We and other research groups have developed radio-luminescent nanomaterials from inorganic and organic building blocks.<sup>10-14</sup> For instance, we previously reported ~500 nm yellow emission from polymer dots (**P-dots**) by using hard X-ray irradiation at a 50-kVp tube voltage with a homoleptic tris-cyclometalated iridium complex.<sup>15</sup> However, the emission color and excitation radiation sources remain limited; thus, it is crucial to further develop these materials in terms of the emission color and radiation source variation.<sup>16</sup> On the other hand, iridium complexes are characterised by changing their luminescent colour and other properties by converting their molecular structure like heteroleptic iridium complexes in various ways, and it was thought that multicolourisation might be possible by changing their structure, compared to organic scintillators such as anthracene. Here, we have developed iridium complex doped **P-dots** that emit over a range of wavelengths and investigated their radioluminescence by using hard X-rays and an electron beam as excitation sources.

### Results and discussion

We synthesized three derivatives of heteroleptic tris-cyclometalated iridium complexes to develop three color variations (**red**, **green**, and **blue**) of iridium complex doped **P-dots** (Fig. 1a and b). **P-dots** are organic nanoparticles composed of polymers and no clear precipitation was observed after synthesis,<sup>17</sup> confirming that their stability is equivalent to that of carbon dots, which have been synthesised frequently recently.<sup>18</sup> Basically, we used three heteroleptic iridium complexes (**Ir-red**, **Ir-green**, and **Ir-blue**) with two cyclometalating bidentate ligands ( $C^N$ ) and one bidentate ancillary ligand ( $N^N$ ), to change the emission color to three primary colors, **red**, **green**, and **blue**. Specifically, **Ir-red** has fluorophenyl quinazoline on the cyclometalating ligands with 2-(2-pyridyl)

<sup>a</sup>SANKEN (The Institute of Scientific and Industrial Research), Osaka University, Mihogaoka 8-1, Ibaraki, Osaka 567-0047, Japan. E-mail: [tosakada@sanken.osaka-u.ac.jp](mailto:tosakada@sanken.osaka-u.ac.jp); [fujii@sanken.osaka-u.ac.jp](mailto:fujii@sanken.osaka-u.ac.jp)

<sup>b</sup>Department of Radiation Oncology and Medical Physics, Stanford University, 300 Pasteur Dr., Stanford, CA 94305, USA. E-mail: [pratx@stanford.edu](mailto:pratx@stanford.edu)

<sup>c</sup>Division of Molecular Science, Graduate School of Science and Engineering, Gunma University, Ota, Gunma 373-0057, Japan

<sup>d</sup>Department of Life Science and Technology, Tokyo Institute of Technology, B-52, 4259 Nagatsuta, Midori-ku, Yokohama, Kanagawa 226-8501, Japan

<sup>e</sup>Innovative Catalysis Science Division, Institute for Open and Transdisciplinary Research Initiatives (ICS-OTRI), Osaka University, 2-1 Yamadaoka, Suita, Osaka 565-0871, Japan

<sup>f</sup>Institute for Advanced Co-Creation Studies, Osaka University, 1-1 Yamadaoka, Suita, Osaka, 565-0871, Japan

† Electronic supplementary information (ESI) available: Materials and general methods. Synthesis of starting compounds, all NMR, and characterization of iridium complex monomers. See DOI: <https://doi.org/10.1039/d3ra01216f>

‡ These authors contributed equally to this work.



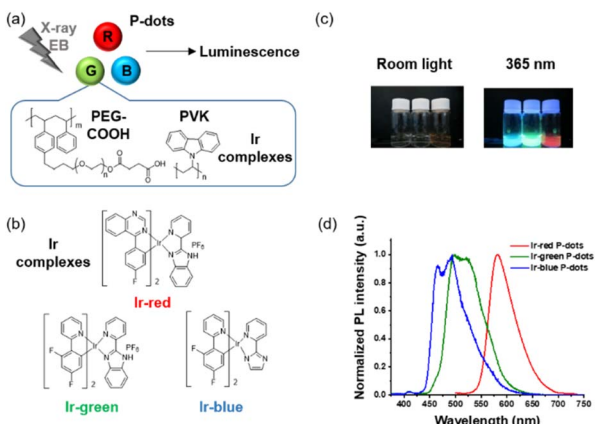


Fig. 1 (a) Schematic of radiation-excited luminescence from **P-dots** doped with iridium complexes. (b) Chemical structures of iridium complexes. (c) Photograph of photoluminescence from **P-dot** solution under room light and 365 nm UV light irradiation. (d) Normalized photoluminescence spectra of **P-dot** solution excited at 365 nm.

benzimidazole (pybi) for the ancillary ligand. **Ir-green** and **Ir-blue** consist of two phenylpyridines with two fluorine functional groups as electron-withdrawing groups on the cyclometalating ligands to stabilize the HOMO level with pybi and 2-(1*H*-imidazol-2-yl)pyridine (pyim) as the ancillary ligand of **Ir-green** and **Ir-blue**, respectively, to change their colors. Compared with pyim, pybi is a  $\pi$ -extended ancillary ligand for stabilizing the LUMO level. **Ir-blue** is neutral, and that **Ir-green** and **Ir-red** are cationic iridium complexes, depending on the synthetic conditions (see ESI<sup>†</sup>). In addition to the emitter design, heteroleptic tris-cyclometalated iridium complexes also meet the following solubility requirement for synthesizing iridium complex doped **P-dots**. The iridium complexes must be soluble in organic solvents such as tetrahydrofuran (THF), but not in water. Subsequently, we selected three appropriate heteroleptic tris-cyclometalated iridium complexes. Detailed synthetic schemes and structural characterizations of the iridium complexes are provided in Fig. S1–S8.<sup>†</sup>

First, we characterized the photochemical properties of these monomeric iridium complexes in organic solvents. The absorption spectra at room temperature are broad in the UV and visible regions (Fig. S9 and Table S1<sup>†</sup>). The photoluminescence spectra excited at 365 nm at room temperature are shown in Fig. S10.<sup>†</sup> The emission maxima and absolute quantum yields of **Ir-red**, **Ir-green**, and **Ir-red** are also listed in Tables S1 and S2.<sup>†</sup> In the presence of dissolved oxygen, the photoluminescence was quenched and the absolute photoluminescence quantum yields dramatically decreased to one-fifth, one-ninth, and one-thirtieth, respectively, for **Ir-red**, **Ir-green**, and **Ir-blue** (Fig. S10<sup>†</sup>). We measured the photoluminescence lifetimes of the iridium complexes in the absence and presence of molecular oxygen (Fig. S11 and Table S3<sup>†</sup>). The quenching rate constants were close to the diffusion-controlled limits of the solvents, suggesting that the triplet excited state is quenched within 1  $\mu$ s. To demonstrate the quenching of the triplet excited state in Ir monomer complexes, we elucidated the triplet excited state of Ir monomer complexes in toluene by

using nanosecond pulse radiolysis, that is a radiation chemistry technique for observing the triplet excited state of organic molecules in aromatic solvents.

The transient absorption spectra of the iridium complexes during pulse radiolysis in toluene are shown in Fig. S12.<sup>†</sup> The absorption maxima at the triplet excited state were at 510, 470, and 440 nm for **Ir-red**, **Ir-green**, and **Ir-blue**, respectively. We also investigated the molecular-oxygen-quenching characteristics of the triplet state by laser flash photolysis (Fig. S13<sup>†</sup>). We observed quenching of the triplet excited state in Ir monomer complexes in organic solvents in accordance with the photoluminescence lifetime measurements (Table S4<sup>†</sup>).

Second, we performed structural characterizations by dynamic light scattering (DLS), zeta potential measurements, and transmission electron microscopy (TEM) (Fig. 2, Tables S5 and S6<sup>†</sup>). DLS measurements indicate hydrodynamic diameters of approximately 100 nm for the three **P-dots** prepared in this study (Table S5<sup>†</sup>). The zeta potential of the **P-dots** was approximately  $-20$  mV, indicating the negatively charged outer surface of the **P-dots** because of the carboxyl groups of the amphiphilic PEG polymers (Table S5<sup>†</sup>). We also observed TEM images to examine their core structures (Fig. 2). The average sizes of the **P-dots** are listed in Table S6.<sup>†</sup> A rough breakdown of the compositional breakdown from the structure results estimated that approximately 5000 Ir complexes and 100 polymers (PVG and PEG together) are doped per particle. The aforementioned results indicate that we successfully synthesized the **P-dots** by co-precipitation.

Third, we investigated photochemical properties of **P-dots**. The photoluminescence and absorption spectra in **P-dots** are shown in Fig. 1c, d, 3 and 4. The photoluminescence colors of **P-dots** were, respectively, red, green, and blue for **Ir-red P-dots**, **Ir-green P-dots**, and **Ir-blue P-dots**, respectively, upon 365 nm light irradiation (Fig. 1c). The photoluminescence quantum yields

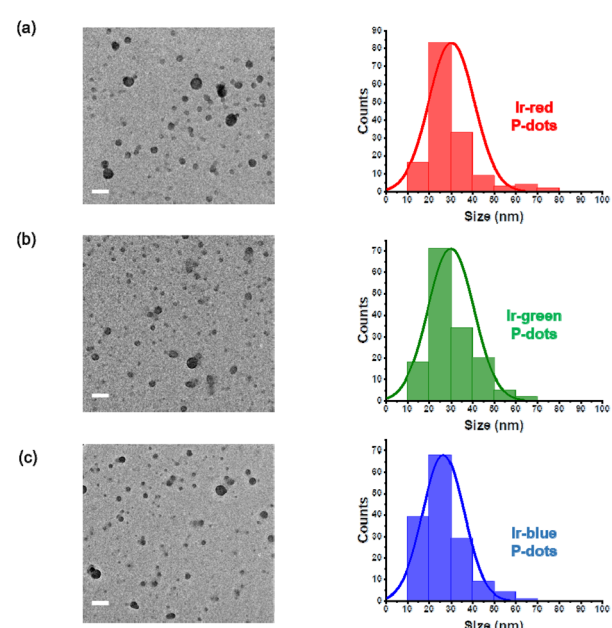


Fig. 2 TEM images and histograms of **P-dots** sizes. (a) **Ir-red P-dots**, (b) **Ir-green P-dots**, and (c) **Ir-blue P-dots**. Scale bar is 100 nm.



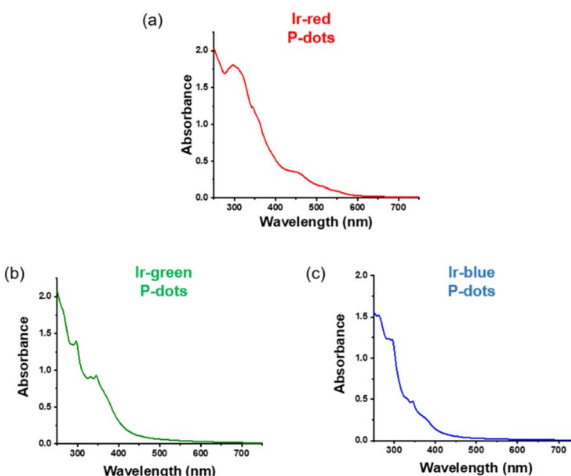


Fig. 3 Absorption spectra of iridium complexes doped P-dots. (a) Ir-red P-dots, (b) Ir-green P-dots, and (c) Ir-blue P-dots.

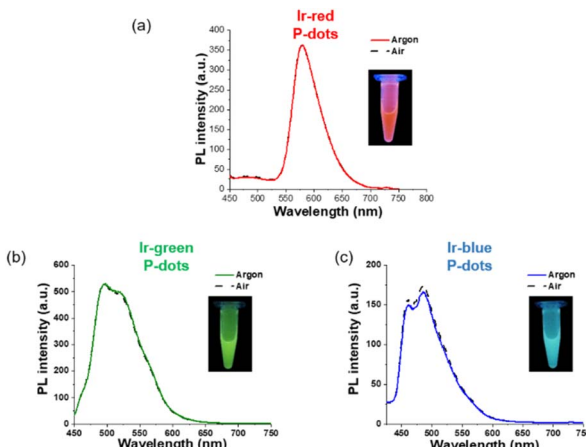


Fig. 4 PL spectra of iridium complex doped P-dots. (a) Ir-red P-dots, (b) Ir-green P-dots, and (c) Ir-blue P-dots, under argon (solid) and air (dashed). The inset shows a photograph of the luminescence of each sample under UV irradiation.

upon UV light irradiation are summarized in Table S2.† The values were smaller than those of corresponding monomeric iridium complexes, but independent of dissolved molecular oxygen. This finding is important for subsequent imaging. We measured the photoluminescence lifetimes of the **P-dots** in the absence and presence of molecular oxygen (Fig. 5 and Table S7†). **P-dots** exhibited photoluminescence lifetime shorter than the corresponding iridium monomeric complexes, probably because of aggregation induced quenching.<sup>19</sup> We also conducted laser flash photolysis by the randomly interleaved pulse train (RIPT) method with a picosecond laser to further investigate the triplet excited state lifetime (Fig. S14†).<sup>20</sup> The lifetime of the triplet excited state was also much shorter than that of the Ir monomer complexes, whereas we were unable to measure **Ir-red P-dots** because of an insufficient detection limit (Table S8†). Regardless, we will conduct a detailed study of this quenching in the future.

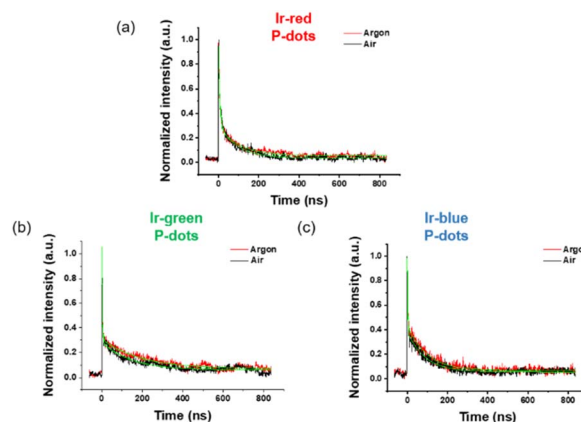


Fig. 5 Lifetime of iridium complex doped P-dots. (a) Ir-red P-dots, (b) Ir-green P-dots, and (c) Ir-blue P-dots under air (black) and argon (red).

These results reconfirm that oxygen has little effect on luminescence in **P-dots**, which is favorable for imaging.

Finally, we investigated luminescence under radiation excitation (Fig. 6a). We placed the samples into a 96-well plate and irradiated them with hard X-rays (60 kVp tube voltage), whereas we observed the luminescence with an electron-multiplying charge-coupled-device (EM-CCD) camera. Hard X-ray beam was directed perpendicularly to the viewing axis, resulting in evident nonuniformity in the emission intensity. We counted the average emission from each well (Fig. 6b). Consistent with the quantum yields of the samples under UV excitation, the **Ir-green** and **Ir-blue P-dots** exhibited more intense luminescence than **Ir-red P-dots** under hard X-ray excitation. We observed the same tendency for the film samples (Fig. 7a). The hard X-ray luminescence spectra of the film samples indicate their emission in the red, green, and blue range (Fig. 7b). In the set-up we used in this study, the spectrum is noisy in **Ir-red P-dots**, but this is probably because the emission itself is so low and close to the detection limit that it was very difficult to obtain a signal itself. We also conducted pulse radiolysis studies to investigate their emission under electron beam irradiation (Fig. 8). We used an electron beam from a linear accelerator (28 MeV) as an excitation source and the resulting luminescence was detected with a multichannel spectroscopic detector. We clearly observed the luminescence spectra during pulse radiolysis (Fig. 8). Under

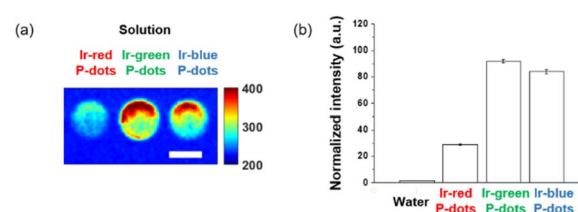


Fig. 6 Hard X-ray excited luminescence of P-dot solutions. (a) X-ray luminescence image. Scale bar is 5 mm. (b) Image intensity quantification of water background, Ir-red P-dots, Ir-green P-dots, and Ir-blue P-dots.



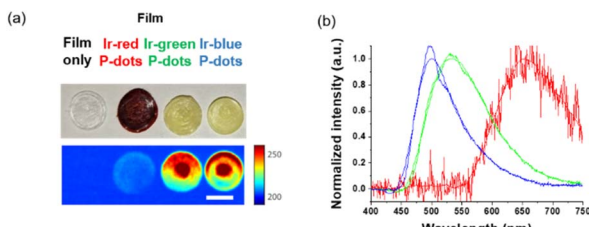


Fig. 7 Hard X-ray excited luminescence of P-dot films. (a) Brightfield photograph (top) and hard X-ray luminescence image (bottom). Scale bar is 7 mm. (b) Hard X-ray luminescence spectra of Ir-red P-dots, Ir-green P-dots, and Ir-blue P-dots embedded in films.

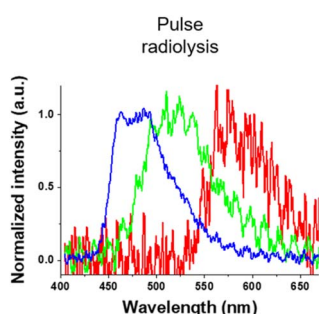


Fig. 8 Luminescence spectra at 0 ns after an electron pulse with a gate time of 500 ns for Ir-red P-dots (red), Ir-green P-dots (green), and Ir-blue P-dots (blue).

radiation excitation, hard X-ray and electron beams ionize  $\text{H}_2\text{O}$  in a manner that forms radicals and ionizing electrons. These ionizing electrons deposit energy into surrounding molecules, leading to further ionization or excitation, the latter of which can result in luminescence. These results clearly indicate that radiation-induced luminescence in visible light wavelengths from **P-dots** doped with heteroleptic tris-cyclometalated iridium complexes. Further mechanistic studies are in progress to understand the origin of the luminescence.

## Conclusions

In this study, we demonstrated color variation of the radio-luminescence from **P-dots** doped with heteroleptic tris-cyclometalated iridium complexes. Consistent with previous studies, the relatively long photoluminescence under UV-visible irradiation is an important consideration for nano-sized scintillators. Here, we confirmed luminescence of three colors upon hard X-ray and electron beam irradiation over a wide range of visible light wavelengths, which is pertinent to further research in imaging and sensing of radiation.

## Experimental section

### Synthesis of P-dots

Iridium complex doped **P-dots** were prepared by co-precipitation.<sup>21</sup> Typically, the iridium complexes and polymers were dissolved in THF at the concentration of  $1 \text{ mg mL}^{-1}$ . Then, the iridium complexes and polymers were diluted in THF to form

a mixture consisting of iridium complexes ( $500 \text{ }\mu\text{g mL}^{-1}$ ;  $5.1 \times 10^{-4} \text{ mol dm}^{-3}$  (**Ir-red**),  $5.5 \times 10^{-4} \text{ mol dm}^{-3}$  (**Ir-green**),  $7.0 \times 10^{-4} \text{ mol dm}^{-3}$  (**Ir-blue**)), PEG ( $5.5 \times 10^{-6} \text{ mol dm}^{-3}$ ) and PVK ( $4.0 \times 10^{-6} \text{ mol dm}^{-3}$ ). The mixture was sonicated to homogeneity. THF solution (0.3 mL) was added into 1 mL of Milli-Q water under sonication. The THF was evaporated by centrifugal evaporation (speed vac.). Finally, water was added to make a final volume of 1 mL to prepare a **P-dot** solution. The prepared **P-dot** solution was stored at  $4^\circ\text{C}$  for immediate use or lyophilized with an FDU-1200 lyophilizer (EYELA, Japan) for storage.

### Preparation of P-dots films

Films were prepared by embedding **P-dots** into polymer matrix. To make polymer matrix, 0.5 g of PVA ( $n = 1700$ , TCI, Japan) was dissolved in 5 mL of Milli-Q water at  $90^\circ\text{C}$  under vigorous stirring. After that, 250  $\mu\text{L}$  of PEG ( $M_w = 200$ , TCI, Japan) was added into PVA solution to form uniform polymer matrix under continuous stirring at  $90^\circ\text{C}$ . The **P-dots** solutions were concentrated 18 times and 1 mL of concentrated **P-dots** solution was mixed with 1 mL of polymer matrix by vigorous stirring to form a uniform mixture. To prepare the films, 200  $\mu\text{L}$  of the polymer mixture was placed on to a polystyrene dish and dried at  $50^\circ\text{C}$ . Then 5 pieces of films were attached together to make thick (1.5 mm) films with a diameter of about 12 mm. The films embedded with **P-dots** were irradiated under hard X-ray for imaging. Film only with PEG and PVA was used for comparison.

### Absolute quantum yield measurements

The absolute quantum yield of **Ir-blue P-dots** and **Ir-green P-dots** were measured with a Quantaurus-QY absolute quantum yield spectrometer (Hamamatsu Photonics K.K., Japan). The sample was measured at the excitation wavelength of 350 nm.

### Photoluminescence lifetime measurements

The time profiles of photoluminescence decay were measured for monomers ( $\text{CH}_2\text{Cl}_2$ ) and **P-dots** ( $\text{H}_2\text{O}$ ) with an EasyLife fluorescence lifetime fluorometer (Optical Building Blocks, NJ, USA). The sample was excited with a 403 nm LED light source equipped with long pass filters; 550 nm for **Ir-red**, 455 nm for **Ir-green**, and 495 nm for **Ir-blue**. The  $\text{O}_2$  effect was studied by degassing under argon flow for 10 min. The rate constant  $k_q$  for  $\text{O}_2$  quenching of the triplet states in the iridium complexes ( $\text{CH}_2\text{Cl}_2$ ) was calculated by:

$$k_{\text{obs}} = k_{\text{TD}} + k_q[\text{O}_2],$$

where  $k_{\text{obs}}$  is the decay constant in air-saturated solution and  $k_{\text{TD}}$  is the decay constant of the triplet state in the absence of  $\text{O}_2$ . The  $\text{O}_2$  concentration in air-equilibrated solution was  $2.2 \times 10^{-3} \text{ mol dm}^{-3}$  in  $\text{CH}_2\text{Cl}_2$  and  $1.9 \times 10^{-3} \text{ mol dm}^{-3}$  in acetonitrile.<sup>22</sup>

### Nanosecond laser flash photolysis for transient absorption measurements of Ir monomer complexes

Nanosecond transient absorption measurement was conducted as previously described.<sup>23</sup> In brief, the sample was irradiated



with a 355 nm Nd<sup>3+</sup>:YAG nanosecond laser (5 ns full width at half maximum) and the transient absorption was probed with multi-channel spectrometer equipped with a pulsed xenon source lamp.

### RIPT method for transient absorption measurements of P-dots<sup>20</sup>

Transient absorption was measured with a picoTAS system at UNISOKU (Hirakata, Osaka).<sup>24</sup> Briefly, a 355 nm picosecond YAG laser (EKSPLA, PL2210A, fwhm 25 ps, 1 kHz, 6 µJ per pulse) was used for excitation.

### Hard X-ray excited luminescence measurements

X-ray luminescence was produced by irradiating the samples with a small-animal X-ray irradiator (X-RAD SmART system, PXI, North Branford, CT, USA) and measured with an EMCCD camera mounted perpendicular to the radiation beam axis. The X-ray beam (60 kVp and 20 mA, unfiltered) was collimated with a 2.5 cm diameter round aperture and directed toward the side of the 96-well plate, each containing 200 µL of sample in solution. We acquired the X-ray luminescence images as series of 20 frames, each taken with a 1 s exposure, an electron gain of 50, and no pixel binning. We used MATLAB (MathWorks, Natick, MA, USA) to remove radiation noise from the raw camera images and quantify the image intensity.

X-ray luminescence spectra were acquired with another X-ray irradiator (PXI XRAD 320, North Branford, CT, USA) and measured with an optical spectrometer (Sensline, Avantes, Lafayette, CO, USA). The X-ray beam (60 kVp and 20 mA, unfiltered) was aimed at the film samples immediately beneath the X-ray aperture to maximize the absorbed dose rate and emitting light intensity. The film samples were placed on top of the distal end of a 1 mm-core-diameter optical fiber whereas the proximal end was coupled to the spectrometer. Each film sample was measured 3× with an exposure time of 5 s each for averaging. The spectra signals were then corrected by subtracting a background signal (non-doped control film) followed by spectral intensity correction to rectify the non-uniform sensitivity of the spectrometer at various wavelengths. The spectra were then normalized and smoothed with a Savitzky–Golay filter in MATLAB.

### Pulse radiolysis for transient absorption and luminescence measurements

Pulse radiolysis was performed with an electron pulse (28 MeV, 8 ns, 0.7 kGy) from the L-band LINAC at SANKEN, Osaka University.<sup>25</sup> An electron beam was used for as the excitation source; transient absorption or luminescence was measured with a multi-channel spectrometer or photomultiplier tube equipped with a monochromator.

### Conflicts of interest

There are no conflicts to declare.

## Acknowledgements

We thank the members of the Radiation Laboratory of SANKEN, Osaka University, for running the linear accelerator and Dr Tatsuo Nakagawa at UNISOKU for the RIPT method on transient absorption measurements of P-dots. This work was partly supported by JSPS KAKENHI Grant Number JP17K19103 and the Initiative for realizing diversity in the research environment project at Osaka University to YO. MY acknowledges a financial support from the Cooperative Research Program “Network Joint Research Center for Materials and Devices”. The authors gratefully acknowledge funding through Stanford Molecular Imaging Scholars (SMIS) Program (NIH T32 CA118681) to HTMN. We thank Michael Scott Long, PhD, from Edanz for editing a draft of this manuscript (<https://jp.edanz.com/ac>).

## References

- 1 C. Dujardin, E. Auffray, E. Bourret-Courchesne, P. Dorenbos, P. Lecoq, M. Nikl, A. N. Vasil'ev, A. Yoshikawa and R. Y. Zhu, *IEEE Trans. Nucl. Sci.*, 2018, **65**, 1977–1997.
- 2 C. Bilynsky, N. Millot and A.-L. Papa, *Bioeng. Transl. Med.*, 2022, **7**, e10256.
- 3 J. Xie, M. Zhao, C. Wang, Y. Yong, Z. Gu and Y. Zhao, *Adv. Healthcare Mater.*, 2021, **10**, 2001615.
- 4 O. Piccolo, J. D. Lincoln, N. Melong, B. C. Orr, N. R. Fernandez, J. Borsavage, J. N. Berman, J. Robar and M. N. Ha, *Sci. Rep.*, 2022, **12**, 1559.
- 5 H. Chen, M. M. Rogalski and J. N. Anker, *Phys. Chem. Chem. Phys.*, 2012, **14**, 13469–13486.
- 6 L. He, X. Yu and W. Li, *ACS Nano*, 2022, **16**, 19691–19721.
- 7 A. F. Bartley, M. Fischer, M. E. Bagley, J. A. Barnes, M. K. Burdette, K. E. Cannon, M. S. Bolding, S. H. Foulger, L. L. McMahon and J. P. Weick, *J. Neural Eng.*, 2021, **18**, 046036.
- 8 Z. Chen, V. Tsytarev, Y. Z. Finfrock, O. A. Antipova, Z. Cai, H. Arakawa, F. W. Lischka, B. M. Hooks, R. Wilton and D. Wang, *ACS Nano*, 2021, **15**, 5201–5208.
- 9 J. Perego, I. Villa, A. Pedrini, E. C. Padovani, R. Crapanzano, A. Vedda, C. Dujardin, C. X. Bezuidenhout, S. Bracco, P. E. Sozzani, A. Comotti, L. Gironi, M. Beretta, M. Salomon, N. Kratochwil, S. Gundacker, E. Auffray, F. Meinardi and A. Monguzzi, *Nat. Photonics*, 2021, **15**, 393–400.
- 10 Q. Chen, J. Wu, X. Ou, B. Huang, J. Almutlaq, A. A. Zhumekenov, X. Guan, S. Han, L. Liang, Z. Yi, J. Li, X. Xie, Y. Wang, Y. Li, D. Fan, D. B. L. Teh, A. H. All, O. F. Mohammed, O. M. Bakr, T. Wu, M. Bettinelli, H. Yang, W. Huang and X. Liu, *Nature*, 2018, **561**, 88–93.
- 11 Z. Liu, K. O. Jung, R. Takahata, M. Sakamoto, T. Teranishi, M. Fujitsuka, G. Pratx and Y. Osakada, *RSC Adv.*, 2020, **10**, 13824–13829.
- 12 D. J. Naczynski, C. Sun, S. Turkcan, C. Jenkins, A. L. Koh, D. Ikeda, G. Pratx and L. Xing, *Nano Lett.*, 2015, **15**, 96–102.
- 13 Y. Osakada, G. Pratx, C. Sun, M. Sakamoto, M. Ahmad, O. Volotskova, Q. Ong, T. Teranishi, Y. Harada, L. Xing and B. Cui, *Chem. Commun.*, 2014, **50**, 3549–3551.



14 C. Sun, G. Pratx, M. Carpenter Colin, H. Liu, Z. Cheng, S. Gambhir Sanjiv and L. Xing, *Adv. Mater.*, 2011, **23**, H195–H199.

15 Y. Osakada, G. Pratx, L. Hanson, P. E. Solomon, L. Xing and B. Cui, *Chem. Commun.*, 2013, **49**, 4319–4321.

16 D.-L. Ma, C. Wu, W. Tang, A.-R. Gupta, F.-W. Lee, G. Li and C.-H. Leung, *J. Mater. Chem. B*, 2018, **6**, 537–544.

17 Y. Osakada, L. Hanson and B. Cui, *Chem. Commun.*, 2012, **48**, 3285–3287.

18 X. Wang, Y. Zhang, J. Li, G. Liu, M. Gao, S. Ren, B. Liu, L. Zhang, G. Han, J. Yu, H. Zhao and F. Rosei, *Small Methods*, 2022, **6**, 2101470.

19 S. Takayasu, T. Suzuki and K. Shinozaki, *J. Phys. Chem. B*, 2013, **117**, 9449–9456.

20 T. Nakagawa, K. Okamoto, H. Hanada and R. Katoh, *Opt. Lett.*, 2016, **41**, 1498–1501.

21 Y. Osakada, T. Fukaminato, Y. Ichinose, M. Fujitsuka, Y. Harada and T. Majima, *Chem.-Asian J.*, 2017, **12**, 2660–2665.

22 M. Montalti, A. Credi, L. Prodi, M. T. Gandolfi and Editors, *Handbook of photochemistry*, 3rd edn, 2006.

23 Y. Osakada, K. Kawai, M. Fujitsuka and T. Majima, *Chem. Commun.*, 2008, 2656–2658.

24 M. Fujitsuka, C. Lu, B. Zhuang, E. Kayahara, S. Yamago and T. Majima, *J. Phys. Chem. A*, 2019, **123**, 4737–4742.

25 Y. Wei, S. Samori, S. Tojo, M. Fujitsuka, J.-S. Lin, C.-T. Chen and T. Majima, *J. Am. Chem. Soc.*, 2009, **131**, 6698–6707.

